

Cartesian Coordinate, Oblique Boundary, Finite Differences and Interpolation

I H Hutchinson

Plasma Science and Fusion Center and
Department of Nuclear Science and Engineering,
Massachusetts Institute of Technology, Cambridge, MA, USA

Abstract

A numerical scheme is described for accurately accommodating oblique, non-aligned, boundaries, on a three-dimensional cartesian grid. The scheme gives second-order accuracy in the solution for potential of Poisson's equation using compact difference stencils involving only nearest neighbors. Implementation for general "Robin" boundary conditions and for boundaries between media of different dielectric constant for arbitrary-shaped regions is described in detail. The scheme also provides for the interpolation of field (potential gradient) which, despite first-order peak errors immediately adjacent to the boundaries, has overall second order accuracy, and thus provides with good accuracy what is required in particle-in-cell codes: the force. Numerical tests on the implementation confirm the scalings and the accuracy.

1 Introduction

For certain types of modeling problem it is advantageous to use cartesian finite-differences on a lattice that does not conform to the interfaces or boundaries of the space under consideration. Instead of the common adoption of an unstructured mesh that conforms to the geometry, the interfaces are considered to be arbitrary surface shapes, and the difference equations are modified adjacent to them to account for their boundary conditions. Such a choice is natural, for example, if the interfaces actually move in time, since then the remeshing cost might become excessive.

One option for cartesian finite difference is to regard the interfaces as being approximated by "staircase" contours that follow cell boundaries. The problem with such a choice is that it constitutes a gross approximation for smooth, possibly curved, diagonal interfaces. In view of the rapidly increasing computational cost of reducing the cell size in multiple dimensions so as to reduce the errors in such a representation, a more attractive option appears to be to accommodate diagonal interfaces with a difference scheme and appropriate interpolation

that is higher order, notably quadratic, in the cell size, but depends as far as possible only on the local values of the potential.

This paper describes a scheme for solving Poisson’s equation with a wide range of general boundary conditions at interfaces, and subsequently interpolating the potential and field (potential-gradient) back to arbitrary points in the solution region. The scheme has been built into a 3-D Particle-in-Cell (PIC) code for solving self-consistent electrostatic plasma problems[1]. Examples to demonstrate the convergence have been studied.

2 One-dimensional differences and interpolation

2.1 Difference approximations

First consider a one-dimensional mesh (not necessarily equally spaced) of nodes x_i on which a potential quantity ϕ is defined. For cells not affected by interfaces, we consider the gradient to be given at positions half-way between nodes, $x_{i+1/2} \equiv (x_i + x_{i+1})/2$, as $\phi'_{i+1/2} = (\phi_{i+1} - \phi_i)/dx_i$, where $dx_i \equiv x_{i+1} - x_i$ and to be interpolated linearly between adjacent values. See Fig. 1. So for cells that are not affected by interfaces, $\phi'(x) = [\phi'_{i+1/2}(x - x_{i-1/2}) + \phi'_{i-1/2}(x_{i+1/2} - x)]/(x_{i+1/2} - x_{i-1/2})$. The second derivative is then $\phi''_i = (\phi'_{i+1/2} - \phi'_{i-1/2})2/(dx_i + dx_{i-1})$, which we note is uniform because this is a second-order interpolation of ϕ . Because ϕ'' is uniform, it introduces no inconsistency to regard the ϕ'' registration as being at position x_i , the same place as ϕ_i , even if the mesh is non-uniform so that x_i is not half way between $x_{i-1/2}$ and $x_{i+1/2}$.

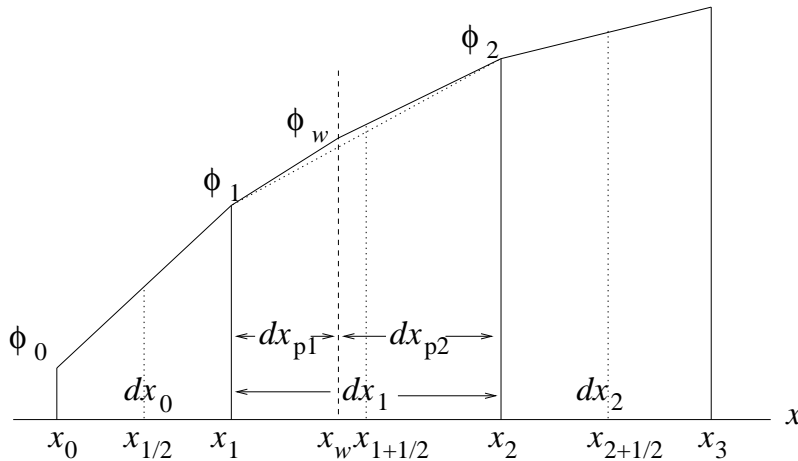


Figure 1: Mesh notation in the vicinity of an interface cutting a cell at x_w .

In order to alleviate notation complexities we consider specifically cell 1 to be cut by an interface (wall) with notation illustrated in Figure 1 at position x_w , where a boundary condition is applied. We will consider the interpolation and solution on the left of the

interface, but the right is (under most conditions) simply the mirror image. We are seeking a solution of the potential on the whole grid: both sides of the interface.

2.1.1 Robin Boundary Condition

The boundary condition to be applied at x_w we will take initially as being given by

$$A\phi_w + B\phi'_w + C = 0. \quad (1)$$

This form, sometimes called the ‘‘Robin’’ boundary condition, accommodates setting the value of ϕ , or ϕ' , or some logarithmic gradient ϕ'/ϕ .

In bulk mesh branches (not affected by interfaces), the value of ϕ''_i applies only up to $x_{i+1/2}$. If an interface intersects the mesh between x_i and $x_{i+1/2}$, as illustrated in Fig. 1, then ϕ''_i applies only up to that interface position, x_w , and ϕ''_i must be evaluated using information from the boundary condition, not x_{i+1} , because x_{i+1} is not part of the solution to the left of the interface. If an interface intersects the mesh between $x_{i+1/2}$ and x_{i+1} , then again calculation of ϕ''_i cannot use x_{i+1} , and also ϕ'' beyond this half-cell position cannot use standard differences and the values at $x_{i+1,2}$ because they are not part of the solution region; so we must make some other assumption. The most natural is to assume that the value ϕ''_i applies right up to the interface, x_w , no matter its distance. Consequently, the second derivative expression,

$$\phi''_1 = \left(\frac{\phi_w - \phi_1}{dx_{p1}} - \frac{\phi_1 - \phi_0}{dx_0} \right) \frac{2}{dx_0 + dx_{p1}}, \quad (2)$$

must be considered to apply right up to x_w . And in particular

$$\phi'_w = \frac{\phi_w - \phi_1}{dx_{p1}} + \phi''_1 \frac{dx_{p1}}{2} = \left[\frac{dx_0 + 2dx_{p1}}{dx_{p1}} (\phi_w - \phi_1) - \frac{dx_{p1}}{dx_0} (\phi_1 - \phi_0) \right] \frac{1}{dx_0 + dx_{p1}}. \quad (3)$$

We then determine ϕ_w and ϕ'_w from a simultaneous solution of (1) and (3), and substitute into (2) to determine the second derivative, which after some algebra can be written:

$$\phi''_1 = \left[\frac{(-C - A\phi_1)}{Adx_{p1} + B} - \frac{\phi_1 - \phi_0}{dx_0} \right] \frac{2}{dx_0 + dx_p}, \quad (4)$$

where

$$dx_p = dx_{p1} \frac{(Adx_{p1} + 2B)}{(Adx_{p1} + B)} \quad (5)$$

can be thought of as the equivalent mesh point distance corresponding to the boundary form. For $B = 0$ (ϕ_w specified) dx_p is dx_{p1} , while for $A = 0$ (ϕ'_w specified) it is $2dx_{p1}$. It can easily be verified that the corresponding expressions for ϕ''_1 are in agreement with intuition. This difference scheme is entirely equivalent to that of Shortley and Weller[2], and subsequently Johansen and Colella[3] (and others), when used with Dirichlet conditions ($B = 0$). These schemes are known to give $\nabla^2\phi$ to first order (truncation is $O(dx)$) for

unequal differences[4, 5], and hence automatically at boundaries. But because the errors are localized at the unequal difference points, the overall solution is generally second-order accurate[6].

Integrating, we obtain the equivalent interpolation:

$$\phi'(x) = \phi'_{1/2} + \phi''_1(x - x_{1/2}), \quad (6)$$

and

$$\phi(x) = \phi_1 + \phi'_{1/2}(x - x_1) + \phi''_1[(x - x_{1/2})^2 - (x_1 - x_{1/2})^2]/2, \quad (7)$$

which can be used to approximate the potential right up to the wall.

Notice that this scheme uses a Taylor-expansion type interpolation, and appears to be the most accurate such scheme (for Laplace's equation or slowly varying second-derivative) that restricts itself to a three-point stencil. The three points are used to deduce three coefficients of the interpolation. Potential and its derivative are continuous except possibly at the wall.

2.1.2 Media Boundary and Surface Charge Condition

A different condition is to take the interface to be the boundary between two dielectric media with dielectric constant ϵ_1 and ϵ_2 . It is simple to generalize this condition to include a specified surface charge density $\epsilon_0\sigma$ such that at the interface, the values in the left and right regions (1 and 2) are related by a jump condition

$$[\epsilon\phi']_2^1 = \sigma. \quad (8)$$

[Thus σ is the *external* charge in excess of any that arises from dielectric polarization.] In order to express this condition symmetrically, we need to extrapolate to get ϕ'_{w1} using (3) but we also need to extrapolate from the right to get the gradient immediately on the other side of the interface ϕ'_{w2} . We do not wish to use an expression corresponding to (3) to the right of the boundary, because that would involve ϕ_3 , and lead to a stencil that extended more than one leg from the node (1) under consideration. Therefore, we make the ansatz that the charge density (i.e. $\epsilon\phi''$) has the same value in region 2 as in region 1. This is consistent with our presumption already made that ϕ'' is uniform on one side in the vicinity of the boundary. The resulting boundary condition is

$$\epsilon_1\phi'_{w1} - \epsilon_2\phi'_{w2} = \left(\epsilon_1 \frac{\phi_w - \phi_1}{dx_{p1}} + \epsilon_1\phi''_1 \frac{dx_{p1}}{2} \right) - \left(\epsilon_2 \frac{\phi_2 - \phi_w}{dx_{p1}} + \epsilon_1\phi''_1 \frac{dx_{p2}}{2} \right) = \sigma \quad (9)$$

which is

$$(\phi_w - \phi_1) \left(\frac{\epsilon_1}{dx_{p1}} + \frac{\epsilon_2}{dx_{p2}} \right) = (\phi_2 - \phi_1) \frac{\epsilon_2}{dx_{p2}} - \epsilon_1\phi''_1 \frac{dx_{p1}}{2} + \sigma. \quad (10)$$

Substituting this $(\phi_w - \phi_1)$ into eq. (2) we find

$$\phi''_1 = \left[\frac{\sigma dx_{p2}/\epsilon_2 + (\phi_2 - \phi_1)}{dx_{p1} + dx_{p2}\epsilon_1/\epsilon_2} - \frac{\phi_1 - \phi_0}{dx_0} \right] \frac{2}{dx_0 + dx_p}, \quad (11)$$

where

$$dx_p = dx_{p1} + dx_1/[1 + (dx_{p1}\epsilon_2)/(dx_{p2}\epsilon_1)]. \quad (12)$$

This gives the difference form and the gradient extrapolation through eqs. (6, 7). It has the merit that when $\epsilon_1 = \epsilon_2$ the differences reduce to those in the absence of an interface, and regardless of the ϵ_1, ϵ_2 values that the sum of the two dx_p values adjacent to either side of the interface is always equal to $2x_1$. Naturally σ gives an extra term representing a charge density.

2.2 Difference Stencils

In order to specify the difference scheme implementation for Poisson's equation

$$\nabla^2\phi = \rho, \quad (13)$$

it is helpful to have explicit formulas for the difference stencil. In the present approach the stencil involves only adjacent points. In N_d dimensions, this choice gives rise to a $(2N_d + 1)$ -point stencil. With reference to Fig. 1, the difference equation at node (1) is written:

$$\left(\sum_{\delta} P_{\delta}\right)\phi_1 - \sum_{\delta} (Q_{\delta}\phi_{\delta}) = \rho_1 + \sum_{\delta} \tau_{\delta}. \quad (14)$$

Here, δ takes on the values corresponding to the adjacent nodes (negative, point 0, and positive, point 2, in the one-dimensional case being illustrated); P_{δ}, Q_{δ} , and τ_{δ} are coefficients that will be specified in a moment. Note that only the sums $\sum_{\delta} P_{\delta}$ and $\sum_{\delta} \tau_{\delta}$ need to be stored in addition to all Q_{δ} . Thus the storage per node required to specify the difference equation is $2N_d + 2$ quantities.

Along the dimension under consideration, the value of the diagonal coefficient is

$$P = \frac{2}{(dx_p + dx_m)d_{eff}}. \quad (15)$$

The $dx_{p,m}$ -quantities can be considered to represent the distances from the node under consideration to the control position in the positive dx_p and negative dx_m directions, and there is an extra effective distance d_{eff} . When there is no boundary, for example when the negative direction is between x_1 and x_0 , then the control distance is to the adjacent node:

$$dx_m = dx_0. \quad (16)$$

In the direction of the boundary, the other quantities are given in table 1, now to be explained.

The "None" condition means a situation where there is no boundary. This row gives the standard coefficients of the difference scheme away from boundaries. The table specifies only the coefficients for the positive δ (point 2 relative to point 1). The coefficients for the negative δ (point 0 relative to point 1) follow from reflectional symmetry. For example for the "None" case the negative side coefficients are given by eq. (15) with $dx_m = dx_1, dx_p = dx_0, d_{eff} = dx_0$.

Boundary Condition	dx_p	d_{eff}	Q	τ
None	dx_1	dx_1	P	0
$A\phi + B\phi' + C = 0$	$\frac{Adx_{p1}+2B}{Adx_{p1}+B}dx_{p1}$	$dx_{p1} + \frac{B}{A}$	0	$-\frac{C}{A}P$
Continuity	$dx_{p1} + \frac{dx_{p2}^2}{dx_{p1}} \frac{B}{Adx_{p2}+B}$	dx_{p1}	$\frac{B}{Adx_{p2}+B}P$	$\frac{-Cdx_{p2}}{Adx_{p2}+B}P$
Media $[\epsilon \frac{\partial}{\partial n} \phi]_2^1 = \sigma$	$dx_{p1} + dx_1 / (1 + \frac{dx_{p1}\epsilon_2}{dx_{p2}\epsilon_1})$	$dx_{p1} + \frac{\epsilon_1}{\epsilon_2} dx_{p2}$	P	$-P\sigma dx_{p2} / \epsilon_2$

Table 1: Coefficients of the difference scheme.

The Robin case, $A\phi + B\phi' + C = 0$, prescribes the condition that applies on the left side of the interface position (i.e. it is what point 1 sees in the positive direction towards point 2). In this case, the value of potential at x_2 is unused, and instead a constant τ contribution is added. It acts like an additional charge density. Together the coefficients of this row are equivalent to equation (4). When there is an interface on the opposite side of the stencil center-point from the coefficients being evaluated, the value of dx_m to be used is equal to dx_p for that opposite direction. In other words, the coefficients for negative δ , in the stencil centered at x_1 , are obtained by taking $dx_p = d_{eff} = dx_0$, and $Q = P$, but $dx_m = \frac{Adx_{p1}+2B}{Adx_{p1}+B}dx_{p1}$.

When a gradient boundary condition is applied using the Robin form with $B \neq 0$, then the boundary condition applied on the other side of the interface is usually just continuity of potential. If any other condition is applied, including the identical Robin condition, then a discontinuity in the potential will arise unless the exterior boundary conditions are consistently chosen. A discontinuity in potential *gradient* is usually physically acceptable (as a surface charge) but a potential discontinuity is usually not. Therefore a ‘‘Continuity’’ boundary condition is provided explicitly in the table to obtain the coefficients for point (2) relative to point (1) for the case where the Robin condition applies on the other side of the interface. That is, when point (2) sees the Robin condition in the direction of point (1) with the prescribed A , B , and C values. Naturally, when $B = 0$, this continuity condition reverts to the fixed- ϕ boundary condition: it becomes identical to the row above it.

The ‘‘Media’’ row documents the stencils needed to implement the treatment explained in section 2.1.2.

3 Multiple Dimensions

The one-dimensional problem just discussed is relatively straightforward. Extension to multiple dimensions requires that a number of important complicating factors be considered.

3.1 Difference Stencil and Boundary Conditions

The difference scheme considered here for the Laplacian in N_d dimensions is based upon the simplest stencil employing only the $2N_d$ adjacent points, giving a $(2N_d+1)$ -point stencil. If

we consider a second-order Taylor expansion about a point that for notational convenience we take to be the origin of coordinates, it may be written:

$$\phi(x_\alpha) = \phi_1 + \sum_{\alpha}^{N_d} p_\alpha x_\alpha + \sum_{\alpha}^{N_d} q_\alpha x_\alpha^2 + \sum_{\alpha}^{N_d} \sum_{\beta > \alpha} r_{\alpha\beta} x_\alpha x_\beta, \quad (17)$$

where α refers to the dimension number and p , q , and r are the expansion's coefficients numbering N_d , N_d , and $N_d(N_d - 1)/2$ respectively. The $2N_d$ differences of the $(2N_d + 1)$ -point stencil permit the determination of only the p_α and q_α in addition to ϕ_1 . The r coefficients, which exist for $N_d > 1$ in increasing numbers, cannot be determined. Fortunately, those cross terms do not contribute to the Laplacian, so that the multidimensional stencil can still determine the Laplacian to the same truncation order, using the 1-D difference scheme for each dimension.

If the boundary conditions are of the Dirichlet type, specifying ϕ , then the generalization essentially straightforward. We use the $B = 0$ version of eq (4) for second derivatives, and stencil contributions, in all coordinate directions. Their sum comprises the Laplacian. Such an approach in two-dimensions is frequently called the ‘‘Shortley-Weller’’ approximation, and is known to be second-order accurate, for essentially the same reasons as for 1-D.

Gradient Boundary Conditions. If, however, we have a full boundary condition at the wall of the form

$$A\phi + B\hat{\mathbf{n}} \cdot \nabla\phi + C = 0, \quad (18)$$

where $\hat{\mathbf{n}}$ is the normal unit-vector, then we need to translate this requirement into an equivalent for each of the dimensions, where wall intersections occur between nodes. It is the presence of the normal gradient $\partial\phi/\partial n$ that is problematic, so Neumann conditions ($A = 0$) experience the same difficulty. Suppose the unit vector for (cartesian) dimension α is $\hat{\mathbf{e}}_\alpha$, and consider an elementary volume (half of a hypercuboid: in 3-D a tetrahedron, see Fig. 2) defined by the planes normal to the dimension axes cut by the wall plane with normal $\hat{\mathbf{n}}$. If the area of the face of this volume defined by the wall plane is Ω , then the area of the face perpendicular to axis- α is $\Omega\hat{\mathbf{e}}_\alpha \cdot \hat{\mathbf{n}}$. Consequently flux conservation demands that $\sum_{\alpha} \hat{\mathbf{e}}_\alpha \cdot \hat{\mathbf{n}} \nabla_{\alpha}\phi = \hat{\mathbf{n}} \cdot \nabla\phi$. Therefore the flux-conservation implicit in the Laplacian is maintained together with eq (18) if in the α -dimension boundary condition,

$$A\phi + B_{\alpha} \nabla_{\alpha}\phi + C = 0, \quad (19)$$

we take $B_{\alpha} = (B/\hat{\mathbf{e}}_{\alpha} \cdot \hat{\mathbf{n}})$, (since $\sum_{\alpha} (\hat{\mathbf{e}}_{\alpha} \cdot \hat{\mathbf{n}})^2 = 1$). This choice amounts to taking $\nabla\phi = \hat{\mathbf{n}}|\nabla\phi|$, and ignores contributions to $\nabla_{\alpha}\phi$ arising from any *tangential* component of the gradient. Such contributions might change the values of $\nabla_{\alpha}\phi$ for individual directions α , but they sum to zero in the normal component. In so far as the control volume adjacent to the boundary can indeed be considered to be half a hypercuboid, the tangential gradient *does not contribute* to the divergence of the flux, because at the interface its normal component is zero and at the lattice cell-boundaries the flux is obtained directly from the finite differences there, regardless of what is the flux tangential to the oblique interface. Thus, for multidimensional

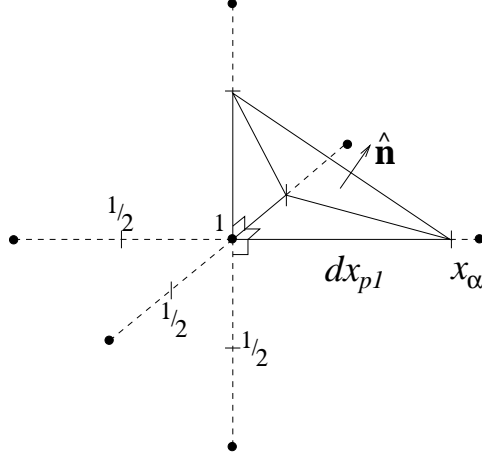


Figure 2: Interface intersecting the lattice legs forming a tetrahedron in 3 dimensions.

evaluation of the Laplacian, in the vicinity of an interface, one can use for each dimension the one-dimensional stencil derived in section 2 but with the boundary condition coefficient $B_\alpha = (B/\hat{\mathbf{e}}_\alpha \cdot \hat{\mathbf{n}})$.

By the same argument, when a surface charge density σ is present, which gives rise to a gradient discontinuity, the fraction of that charge density to be attributed to dimension α is $\hat{\mathbf{e}}_\alpha \cdot \hat{\mathbf{n}}$. Then, associated with an interface area Ω , dimension α possesses a projected area $\Omega \hat{\mathbf{e}}_\alpha \cdot \hat{\mathbf{n}}$. When each dimension area is multiplied by its charge density $\hat{\mathbf{e}}_\alpha \cdot \hat{\mathbf{n}} \sigma$ and the resultant summed over all dimensions, the total surface charge $\Omega \sigma$ results. A lattice leg along the α dimension intersecting the surface must use the 1-dimensional difference scheme of eq. (11), but with charge density $\hat{\mathbf{e}}_\alpha \cdot \hat{\mathbf{n}} \sigma$.

These choices are the appropriate ones for a difference scheme with a $(2N_d+1)$ -point stencil in N_d -dimensions. With the standard expression for the second derivative along each dimension or its generalizations, eqs. (4) or (11) in hand, (as summarized in Table 1) one can then solve the resulting matrix equation by standard methods such as SOR or conjugate gradient minimization, to find the potential on the mesh.

3.2 Multidimensional Interpolation

More complex mathematical considerations and by far the more difficult coding challenges lie in the back-interpolation of the solution to arbitrary position, rather than the solution of the difference equations.

Gradient interpolation. For the dynamics of particles moving in the field, the gradient of the potential is the most important. *Gradient interpolation* is done most naturally using the information embedded in the difference stencils. For gradients in direction α at positions along α -lattice-legs, i.e. at coordinate values in the other dimensions corresponding to a node, the 1-D interpolation is entirely natural and straightforward. Eq. (6) with eq. (4) at

bulk nodes and Dirichlet boundaries, or with eq. (11) at Media and surface-charge interfaces can be used.

However, at interfaces where the Robin (with $B \neq 0$) or any normal-gradient condition is applied, interpolation that sets the tangential gradient to zero is insufficient. It is sufficient for evaluating the Laplacian to ignore tangential gradient but not for the field interpolation. We must estimate the tangential gradients ($N_d - 1$ quantities). We wish to do this for convenience and compactness *without* extending our consideration beyond the standard $(2N_d + 1)$ stencil node values. We therefore have to drop cross-gradients from the Taylor expansion as we do in the bulk scheme. That means we can ignore the normal derivative of the tangential gradients, and determine the gradients on the opposite side of the central node from the interface intersections. That is (see Fig. 2) from the gradients at positions $x_{\alpha,1/2}$, taking the tangential field to be simply constant for the cell under consideration. The estimate of the tangential gradient is therefore

$$\nabla_t \phi = \nabla \phi|_{1/2} - (\hat{\mathbf{n}} \cdot \nabla \phi|_{1/2}) \cdot \hat{\mathbf{n}} \quad (20)$$

(where an appropriate interpolation for $\hat{\mathbf{n}}$ is used if curvature is present). Then when the interface boundary condition is the specification of $\frac{\partial \phi}{\partial n}$, the gradient at each of the face points (dx_{p1}) is

$$\nabla \phi|_w = \nabla_t \phi + \frac{\partial \phi}{\partial n} \hat{\mathbf{n}} = \nabla \phi|_{1/2} - (\hat{\mathbf{n}} \cdot \nabla \phi|_{1/2}) \cdot \hat{\mathbf{n}} + \frac{\partial \phi}{\partial n} \hat{\mathbf{n}}. \quad (21)$$

For direction α , therefore,

$$\phi'_{\alpha w} = \left. \frac{\partial \phi}{\partial x_\alpha} \right|_w = \frac{\phi_1 - \phi_{\alpha 0}}{dx_{\alpha 0}} - n_\alpha \left(\sum_\beta^{N_d} n_\beta \frac{\phi_1 - \phi_{\beta 0}}{dx_{\beta 0}} - \frac{\partial \phi}{\partial n} \right). \quad (22)$$

Substituting for $\frac{\partial \phi}{\partial n}$ from the Robin condition we get

$$\phi'_{\alpha w} = -n_\alpha (A/B) \phi_w - n_\alpha \left(C/B + \sum_\beta^{N_d} n_\beta \frac{\phi_1 - \phi_{\beta 0}}{dx_{\beta 0}} - \frac{\phi_1 - \phi_{\alpha 0}}{n_\alpha dx_{\alpha 0}} \right). \quad (23)$$

This is now in the form of a Robin condition in the single (α) dimension, but with new Robin coefficients

$$A' = A, \quad B' = B/n_\alpha, \quad C' = C + B \left(\sum_\beta^{N_d} n_\beta \frac{\phi_1 - \phi_{\beta 0}}{dx_{\beta 0}} - \frac{\phi_1 - \phi_{\alpha 0}}{n_\alpha dx_{\alpha 0}} \right). \quad (24)$$

These primed coefficients can be substituted into our prior expression for the second derivative, eq (4), to obtain:

$$\phi''_{\alpha 1} = - \frac{\left[C + A\phi_1 + A(\phi_1 - \phi_{\alpha 0}) \frac{dx_{\alpha p 1}}{dx_{\alpha 0}} + B \sum_\beta^{N_d} n_\beta \frac{\phi_1 - \phi_{\beta 0}}{dx_{\beta 0}} \right]}{A dx_{\alpha p 1} + B/n_\alpha} \frac{2}{dx_{\alpha 0} + dx_p}, \quad (25)$$

where $dx_p = dx_{\alpha p 1} (An_\alpha dx_{\alpha p 1} + 2B) / (An_\alpha dx_{\alpha p 1} + B)$. It is helpful to note that in the limits $B \rightarrow 0$, or $n_\alpha \rightarrow 1$ this expression is identical to (4). For other parameters, the most important extra distinction is the inclusion of the B term in the numerator, which involves values $\phi_{\beta 0}$ off the α -lattice-line.

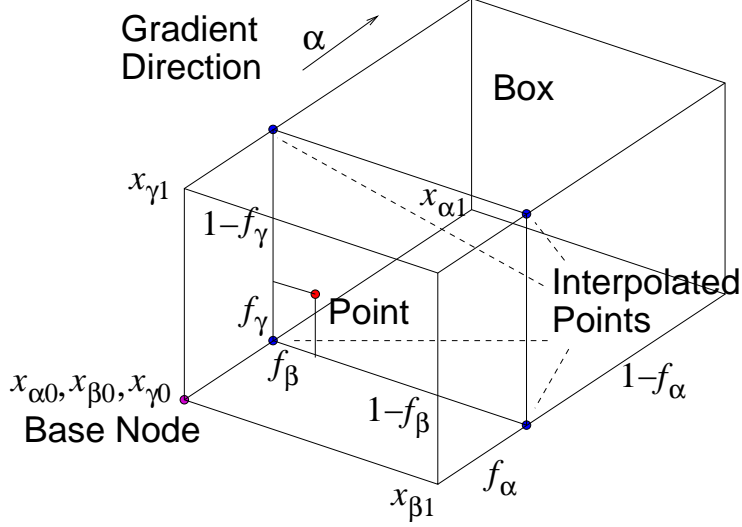


Figure 3: Gradient-interpolation geometry within an elementary lattice box.

Transverse interpolation Referring to Fig 3 which shows an example in 3 dimensions, we use as base the node closest to the point, and the “box” consisting of the elementary cuboid whose vertices are adjacent mesh nodes, in which the point lies.

For the gradient along the α -direction, we use the quadratic interpolation, eq (6), along each of the 2^{N_d-1} lattice legs (i.e. box edges) aligned along the α -direction, to obtain the gradients at interpolated points where the α -coordinate is x_α , a fraction f_α of the lattice spacing from the base, and the other coordinates correspond to nodal values. Then we use multilinear interpolation between those values in the orthogonal (N_d-1) -dimension subspace to approximate the gradient at the point. Multilinear interpolation can be considered to be defined inductively via

$$\phi'(x_\alpha, x_\beta, \dots, x_\eta, \dots, x_{N_d}) = f_\eta \phi'(x_\alpha, x_\beta, \dots, x_{\eta 0}, \dots, x_{N_d}) + (1 - f_\eta) \phi'(x_\alpha, x_\beta, \dots, x_{\eta 1}, \dots, x_{N_d}) \quad (26)$$

for all $\eta \neq \alpha$. It has the important merit of giving continuity at cell boundaries but requiring only localized box information. This scheme provides gradient (field) estimates that are continuous and have at least first order accuracy.

If at the first, quadratic, stage we find a node from which we would do interpolation, e.g. $(x_{\alpha 0}, x_{\beta 1}, x_{\gamma 0})$, to be outside the point’s solution region, i.e. on the other side of an interface, then we examine the other end of the lattice leg under consideration $(x_{\alpha 1}, x_{\beta 1}, x_{\gamma 0})$. If that end lies in the point’s region, then we extrapolate from that instead. If that second end does not lie in the point’s region either, then the lattice leg is entirely outside the interpolation region. In that case, an “over-extrapolation” is sought by looking one more node in either direction. If a node is found that is in the region, then (over-)extrapolation from that node to the lattice position under consideration is adopted. Such a value is considerably more uncertain than values corresponding to points that are in the region or directly extrapolated from the region. Over-extrapolated values are given a weight w equal to one minus the

fractional position relative to the lattice end adjacent to the region. That is, if position $x_{\alpha 0}$ is in the region, and $x_{\alpha 1}$, $x_{\alpha 2}$ not, then the weight at x such that $x_{\alpha 1} < x < x_{\alpha 2}$ is $w(x) = 1 - (x - x_{\alpha 1}) / (x_{\alpha 2} - x_{\alpha 1})$. If there is no extrapolation available, then the weight is set to zero.

When one or more of the weights in a multilinear interpolation is not unity, a weighted multilinear interpolation is used. It can be expressed as a sum over all the $2^{(N_d-1)}$ dimensional corners of the box within which the interpolation is being done, denoted by the vector index whose components have the values $i_\eta = 0$ or 1 , where $1 \leq \eta \leq N_d - 1$ denotes the dimension. Thus

$$\phi' = \sum_{i_\eta=0,1} A(i_\eta) \phi'(i_\eta) / \sum_{i_\eta=0,1} A(i_\eta) \quad \text{where} \quad A(i_\eta) = w(i_\eta) \prod_{\eta} (1 - i_\eta + f_\eta(2i_\eta - 1)). \quad (27)$$

When all $w = 1$, this expression is equivalent to eq (26).

For concave interfaces, it is theoretically possible for a particle to be in a box which has no vertices in its region. If that happens, a fall-back is needed, the natural thing is to choose as base node the nearest node that is in its region. This problem can usually be avoided by choice of mesh in relation to objects.

Potential interpolation. Because we do not directly differentiate the potential, using instead the gradient interpolation just explained, satisfactory values for the potential are obtained by multilinear interpolation, and do not require higher order interpolation schemes. Multilinear interpolation is unproblematic in the “bulk” where all the box vertices are valid points in the relevant region of the grid, and no interface crossings occur on its edges. The problematic issue is how to extrapolate to the interface, when box vertices are absent from the valid region because they are the other side of an interface. After some experimentation, the following approach was found to work well using modest computational resources. First, all the vertices of the box are examined. If any do not lie in the region, they must be filled in with extrapolated values. The extrapolated values are obtained by calculating (during this examination) the centroid, the mean value, and the mean gradients of the “valid” vertices of the box (ones that lie in the region). Additional steps must be taken for any dimension in which the gradient is undetermined, which happens when all the valid vertices have the same coordinate in that dimension. Such a situation occurs when an entire face of the box is outside the valid region. The occurrence is not all that unusual. In such a situation of undetermined gradient, we instead determine the gradient in that dimension, using the gradient interpolation code, evaluated at the point. The values that are filled in to the invalid vertices are then the mean cell value plus the dot product of the gradient and the vector to the vertex from the centroid. Multilinear interpolation can then proceed as usual on the entire box including the filled-in vertices.

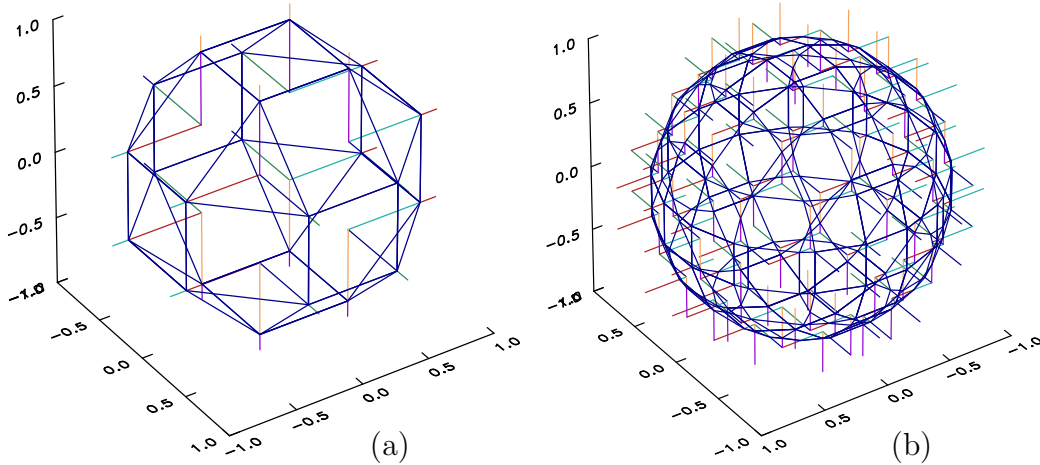


Figure 4: Representation of spherical object on 16^3 (a) and 32^3 (b) grids.

4 Example Accuracy Tests

Here we give examples of the typical accuracy of the difference solution and interpolation schemes. The case illustrated is of a sphere of fixed potential 10, radius 1, inside a second sphere of radius 5 at which the potential logarithmic radial gradient is -1. It is solved on a mesh over the region $-5 \leq x, y, z \leq 5$. The inner sphere wireframe is shown in Fig. 4 for two grids, 32^3 and 16^3 . Also shown in this figure are the lattice legs which are intercepted by the sphere. The wireframe nodes are those intercepts.

The solution of this problem: $\nabla^2 \phi = 0$, is of course $\phi = \phi(1)/r$. In Fig. 5 the values at

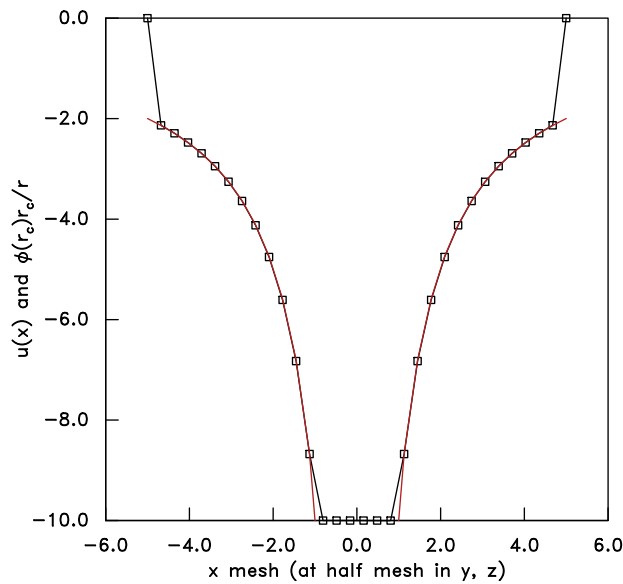


Figure 5: Solution of the difference equation.

the nodes in the plane of constant y, z (through the center) are compared with this analytic

solution. Inside the inner sphere the potential is constant, dictated by continuity at the interface, as would occur for a conducting sphere. (Outside the outer sphere the potential is set to zero.)

The values at the mesh nodes tell only the accuracy of the solution representation at the nodes. Of more interest is the overall accuracy of the solution when interpolated to positions *away* from the nodes. Fig. 6 illustrates this by performing the interpolations previously described along a line of constant direction in the $z = 0$ plane whose angle is 0.1 radians (5.7°) to the x -axis. The lines labelled “getpotential” and “getfield” are the

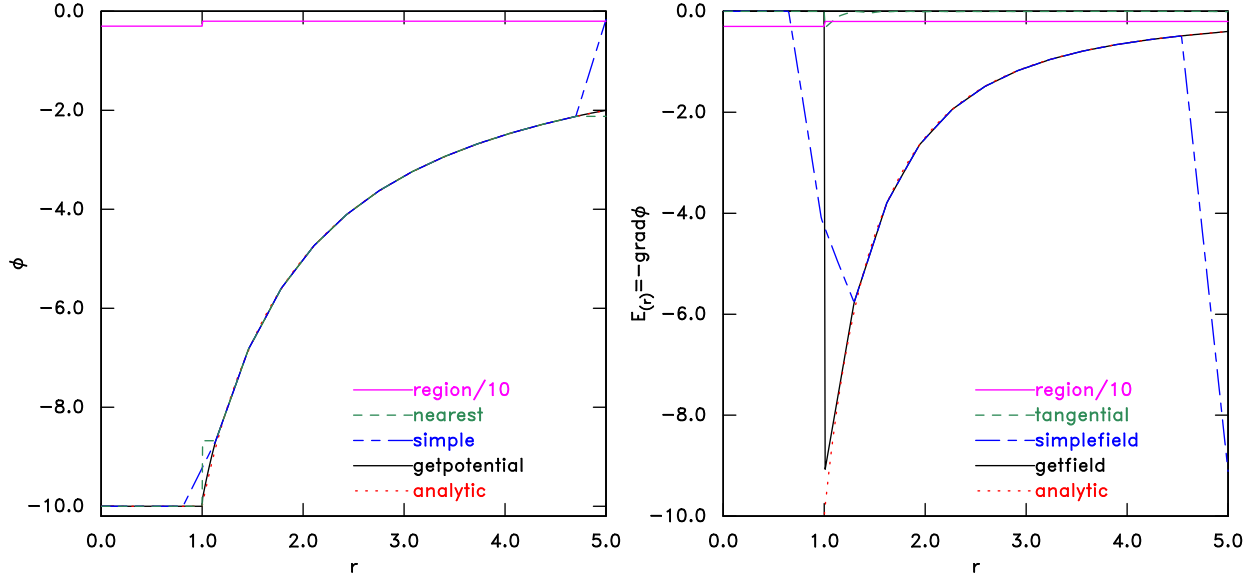


Figure 6: Comparison of different interpolation schemes for 32^3 mesh.

quadratic interpolations. For comparison, the analytic solution is plotted and two other types of approximation. That called “nearest” simply takes the potential to be the value at the nearest node of the mesh. The approximation called “simple” is arrived at by a simple linear interpolation of ϕ between nodes, and for “simplefield” a linear interpolation of $\nabla\phi$ based on taking differences of the ϕ nodal values. The “simple” ϕ and $\nabla\phi$ estimates therefore ignore the extra information embedded in the boundary conditions. We notice that although the ϕ interpolation in the bulk region is very good for all approaches, near the boundaries there are big errors for the simple and nearest approximations. For the getpotential interpolation, the errors are an order of magnitude smaller, having a maximum error of 0.145 along this line, occurring at a position just outside the inner sphere. This value is typical. (The “region/10 line” simply indicates the different regions of the solution.)

The field ($\nabla\phi$) interpolation shows even larger errors in the simple estimate, because linearly interpolating it from differences in the vicinity of its discontinuity at $r = 1$ produces a piecewise linear continuous behavior that is far from the analytic form. The quadratic interpolation *using the boundary information*, by contrast, accommodates the discontinuity in field and obtains very respectable approximations even in the vicinity of the boundary.

The maximum field error varies substantially with the angle of the path. In this case it is about 0.8 in radial field component and less in tangential field.

Figure 7 documents the spatial dependence of the error in the x -direction field in a plane $y = \text{constant}$ ($y \approx 0$). The contours of error are spaced by 0.2. The positions of the nodes

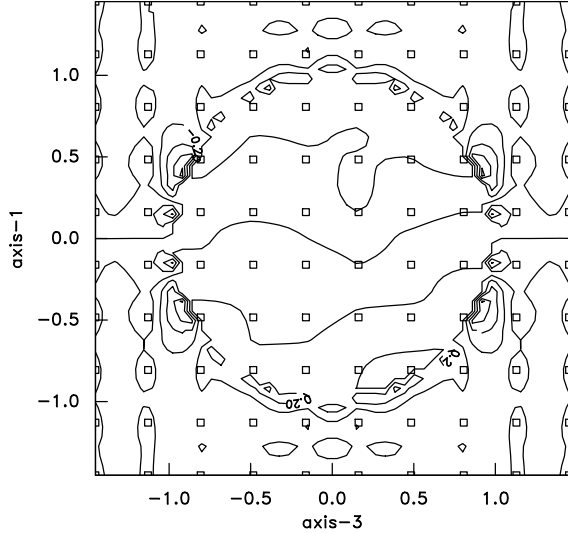


Figure 7: Error in field component in direction-1 within a plane of constant y (axis-2). Contour spacing 0.2. (The maximum of $|\nabla\phi|$ is 10; so contours are 2% relative error.)

are marked by squares. What we see is that the field error is less than 0.2 over most of the domain but locally near the field discontinuity at $r = 1$ larger errors occur that depend upon position round the boundary.

The scale length of the field and potential variation immediately outside $r = 1$ is 1; the mesh spacing is about 0.3. It is therefore evident that we are obtaining highly favorable accuracy, typically 10% maximum local error and 1% standard deviation, in field even with rather coarse mesh resolution (0.3) of the scale-length. Moreover using the boundary information we completely avoid pollution of the field in one region by values in another where it is different by a discontinuity.

Nodes	16^3	32^3	48^3	64^3	128^3
Spacing dx/r_s	0.63	0.31	0.21	0.156	0.078
$\Delta\phi_{max}/\phi_{max}$	0.020	0.0031	0.0014	0.0008	0.0002
$\Delta E_{max}/E_{max}$	0.167	0.091	0.068	0.050	0.022
$SD(\Delta E)/E_{max}$	0.020	0.0089	0.0060	0.0022	0.0007

Table 2: Nodal-potential and field-interpolation relative error scaling with mesh size.

Table 2 show the maximum nodal (i.e. uninterpolated) potential error $\Delta\phi_{max}/\phi_{max}$, and the maximum local (interpolated) field error $\Delta E_{max}/E_{max}$ and standard deviation of the

error $SD(\Delta E)/E_{max}$ evaluated over a central cube of side length 3. These errors decrease with the mesh spacing, as the number of nodes is increased. The nodal potential error decreases quadratically with mesh spacing as expected for this second order scheme. The maximum interpolated field error decreases only linearly, but the error becomes more and more localized so that the standard deviation decreases approximately quadratically. By comparison, the unsatisfactory “simple” interpolation (not shown in the table) gives local field errors whose maximum magnitude is independent of mesh spacing. The “getfield” interpolation asymptotic *scalings* are the same as a “nearest” value interpolation (using the nearest value of the gradient that is based on values only from nodes on the same side of any boundary as the point being interpolated). This is presumably because there are situations near boundaries where the multilinear interpolation provides no tangential-field derivative-information, omitting nodes that lie across a boundary. The *magnitude* of getfield’s error, however, is smaller by a substantial factor (perhaps 3 or 4) than a nearest value approximation, and the volume of its region of bad approximation is smaller.

In summary, using a compact difference stencil, Poisson solution and interpolation of the electric field is implemented with excellent accuracy and convergence, suitable for use in particle in cell codes with purely cartesian mesh but essentially arbitrary oblique boundaries.

References

- [1] I. H. Hutchinson, Phys. Plasmas **18**, 032111 (2011).
- [2] G. H. Shortley and R. Weller, J. Applied Physics **9**, 334 (1938).
- [3] H. Johansen and P. Colella, J. Comp. Phys. **147**, 60 (1998).
- [4] J. H. Bramble and B. E. Hubbard, Numerische Mathematik **4**, 313 (1962).
- [5] Z. Jomaa and C. Macaskill, J. Comp. Phys. **229**, 3675 (2010).
- [6] N. Matsunaga and T. Yamamoto, J. Comp. Appl. Math. **116**, 263 (2000).